six-membered C-atom rings to approach a common geometry. This left just 11 unrestrained degrees of freedom in the description of the local coordinates.

The axis of the pseudo-2/*m* disordering was refined by allowing the orientations of axis systems $P = 3$ and 6 to refine independently. The rotational adjustments of axis systems $Q = 1$ and 2 covary with the rotational adjustments of axis system $P = 3$ and the rotational adjustments of axis systems $Q = 4$ and 5 covary with the rotational adjustments of axis system $P = 6$. It is necessary to impose rotational constraints $\epsilon_1(1) = \epsilon_1(2)$, $\epsilon_2(1) = \epsilon_2(2)$, $\epsilon_3(1) = -\epsilon_3(2)$ and $\epsilon_1(4) = \epsilon_1(5)$, $\epsilon_2(4) = \epsilon_2(5)$, $\epsilon_3(4) = -\epsilon_3(5)$ to remove the redundant degrees of freedom. Non-zero values correspond to distortions that misalign the ring systems. The origin shifts for axial systems $Q = 1$, 2 (and 4, 5) control the positions of the molecules and the —CH=N— linkages between the halves of each molecule. The two angles and one distance of this linkage were restrained to be the same for each molecule by restraining distance differences between molecules to approach zero. Thus, 24 rotation–translation degrees of freedom effectively reduce to 21. For ClMe, the effective degrees of freedom were further reduced by restraining the CH=N distance to be the same as for the MeCl structure and making $\epsilon_1(1) = \epsilon_1(2) = 0$ and $\epsilon_1(4) = \epsilon_1(5) = 0$.

References

BAR, I. & BERNSTEIN, J. (1977). *Acta Cryst.* B**33**, 1738–1744.
BAR, I. & BERNSTEIN, J. (1982). *Acta Cryst.* B**38**, 121–125.
BAR, I. & BERNSTEIN, J. (1983). *Acta Cryst.* B**39**, 266–272.
BERNSTEIN, J. & IZAK, I. (1975). *J. Cryst. Mol. Struct.* **5**, 257–266.
BERNSTEIN, J. & IZAK, I. (1976). *J. Chem. Soc. Perkin Trans.* 2, pp. 429–432.
BERNSTEIN, J. & SCHMIDT, G. M. J. (1972). *J. Chem. Soc. Perkin Trans.* 2, pp. 951–955.
BERNSTEIN, J., BAR, I. & CHRISTENSEN, A. (1976). *Acta Cryst.* B**32**, 1609–1611.
BERNSTEIN, J., ENGEL, M. & HAGLER, A. T. (1981). *J. Chem. Phys.* **75**, 2346–2353.
MEULENAER, J. DE & TOMPA, H. (1965). *Acta Cryst.* **19**, 1014–1018.
RAE, A. D. (1975). *Acta Cryst.* A**31**, 560–570.
RAE, A. D. (1976). *Acta Cryst.* A**32**, 895–897.
RAE, A. D. (1984). *Acta Cryst.* A**40**, C-428.
RAE, A. D. (1992). *RAELS92. A Comprehensive Constrained Least Squares Refinement Program.* Australian National Univ., Australia.
WELBERRY, T. R. & BUTLER, B. D. (1994). *J. Appl. Cryst.* **27**, 205–231.
WELBERRY, T. R., BUTLER, B. D. & HEERDEGEN, A. P. (1993). *Acta Chim. Hung.* **130**, 327–345.

Acta Cryst. (1995). B**51**, 197–209

Electron Density Study by X-ray and Neutron Diffraction of an NLO Compound: *N*-(4-Nitrophenyl)-L-prolinol. Description of Quadratic Hyperpolarizability

BY ABDALLAH FKYERAT, ABDELHALIM GUELZIM AND FRANÇOIS BAERT*

Laboratoire de Dynamique et Structure des Matériaux Moléculaires, CNRS URA 801, *Université des Sciences et Technologies de Lille Flandres Artois,* 59655 *Villeneuve d'Ascq CEDEX, France*

WERNER PAULUS AND GERNOT HEGER

Laboratoire Léon Brillouin CEN Saclay, 91191 *Gif-sur-Yvette CEDEX, France*

AND JOSEPH ZYSS AND A. PÉRIGAUD

Département d'Electronique Quantique et Moléculaire, Laboratoire de Bagneux, CNET, 196 *Avenue Henri Ravera,* 92220 *Bagneux, France*

(*Received* 5 *December* 1993; *accepted* 26 *September* 1994)

Abstract

The study of the electron density and the determination of the dipolar moment of the molecule in the crystalline compound *N*-(4-nitrophenyl)-L-prolinol have been completed using X-ray and neutron diffraction. The deformation maps and the calculations of the atomic net charges demonstrate the character of the donor–acceptor couple (*DA*) linked to the phenyl transmitter. The dipolar molecular moments obtained by several methods have similar values, except the method of kappa refinement. The kappa refinement appears inadequate to solve the phase problem. Accurate knowledge of the first molecular moment reduces the ambiguity on the quadratic polarizability coefficient β, measured from electric field-induced second-harmonic generation (EFISHG). The coefficients of the cubic moment (third-order semi-invariant) of the electronic distribution in the crystal state are compared with those of the quadratic hyperpolariz-

* Author to whom correspondence should be addressed.

ability obtained by theoretical calculations. An estimate of relevant coefficients in octupolar-type materials would provide guidance to the choice of systems for non-linear optics. Crystal data: $C_{11}H_{14}N_2O_3$, $M_r = 222.2$, monoclinic, $P2_1$, $Z = 2$, $F(000) = 236$, $T = 122$ K, $a = 5.152$ (4), $b = 14.790$ (3), $c = 7.134$ (2) Å, $\beta = 106.14$ (4)°, $V = 522.18$ Å^3, $D_x = 1.41$ Mg mm^{-3} at 122 K, $\mu = 0.084$ mm^{-1} for $\lambda = 0.7107$ Å.

Introduction

Non-linear optics has been a topic of intense work in recent years. This can be explained by two main factors: the needs of the telecommunication industry for high band-width optical switching and processing devices necessary to achieve information and data transmission with the high standards required in our computer age; and the rapid development of sophisticated laser tools, which has played an essential role in the research on new methods to monitor single laser pulses used in state-of-the-art non-linear dynamics experiments.

Molecular engineering has led to the development of organic crystals displaying comparable or even better non-linear optical properties than known inorganic materials. Molecules of these materials (*e.g.* nitropyridines with donor and acceptor substitution at *para*-positions) possess correlated and highly delocalized π-electron states. The second-harmonic generation (SHG) in *N*-(4-nitrophenyl)-L-prolinol (NPP) is two orders of magnitude larger than in KDP (Ledoux & Zyss, 1982). Organic materials consist of chemically bonded molecular units interacting in bulk by weak van der Waals forces. In this type of material, the non-linear optical response can be explained primarily by an anharmonic distortion of the electron density distribution inside the molecules due to the intense electric field of an applied optical pulse. Hence, the crystal spectrum will be entirely dependent on the molecular absorption spectrum. The polarizability of the crystal can be calculated using the molecular polarizability, given that the molecular arrangement in the unit cell is known. Up to now, the search for efficient organic materials was directed towards the engineering of molecules with large non-linear responses measured by EFISHG, or calculated by semi-empirical methods based on finite fields (Zyss, 1979*a*,*b*,*c*), or the sum over states [SOS (Lalama & Garito, 1979; Docherty, Pugh & Morley, 1985)].

Since the development of sufficiently compact parametrized descriptions of molecular densities about 20 years ago, accurate experimental measurement of the charge density in a crystal has been feasible (Stewart, 1973). One of the most exciting applications of such an analysis is the evaluation of the one-electron properties in molecular crystals. In a pioneering paper, Coppens, Guru Row, Leung, Stevens, Becker & Yang (1979) demonstrated the feasibility of this procedure for a number of centrosymmetric crystals. However, application to non-centrosymmetric materials, such as organic crystals with non-linear optical applications, has been slow to emerge. This is certainly partly due to the increased difficulty of obtaining accurate model structure factors when the phase is a continuous variable. Nevertheless, recent applications have demonstrated the usefulness and potential accuracy of the technique in the non-centrosymmetric case (Souhassou, Lecomte, Blessing, Aubry, Rohmer, Wiest, Benard & Marraud, 1991). The polarization P induced in a molecule by a local electric field can be expanded in a power series of the electric field

$$P = \mu + \alpha E + \beta : EE + \gamma : EEE + \ldots . \qquad (1)$$

This expression defines the molecular polarizability tensors α, β and γ.

The present study of the charge distribution and the one-electron properties (dipole, quadrupole and octupole moments) in a proven non-optical material, *N*-(4-nitrophenyl)-L-prolinol (NPP), will show that interesting results can be obtained. The accurate determination of the first molecular moment provides a good evaluation of the molecular dipole of the molecule in the crystal, generally in good agreement with the value measured in solution. This first estimate reduces the uncertainty on the quadratic polarizibility coefficient β, measured from EFISHG experiments. Furthermore, the octupole moment of the molecular electron distribution in the crystal state, which is connected to the components of the β-tensor, should yield valuable indications on optical properties. Such a connection is indeed provided by a model developed by Robinson (1967), which will be discussed later in this study.

Experimental

Yellow crystals of NPP, crystallized during the Crocodile space experiment (Perigaud, Gonzales & Cunisse, 1991), have been provided by the CNET. Single NPP crystals, even of small size, are difficult to obtain; the samples used were of a high quality. Gel growth techniques (Andreazza, Josse, Lefaucheux, Robert & Zyss, 1992) were also initiated to grow highly non-linear NPP crystals of larger size. A crystal of $0.45 \times 0.32 \times 0.21$ mm was used to measure Mo $K\alpha$ X-ray diffraction data on an Enraf–Nonius CAD-4 diffractometer equipped with a liquid nitrogen vapour-stream low-temperature apparatus. Diffraction experiments were performed at 122 K (0.5). Cell parameters were determined from refinement using centred angular positions of 25 reflections with $25 < 2\theta < 35°$. The homegeneity of the beam from the graphite incident-beam monochromator was measured with a pinhole of 20 μm, the intensity varied by less than 3.5% over the area intercepted by the specimen crystal. Measurements covered half a sphere with $-10 < h < 10$, $-34 < k < 34$, $0 < l < 15$.

Table 1. *Experimental data for N-(4-nitrophenyl)-L-prolinol*

Parameter	X-ray	Neutron
a (Å)	5.152 (4)	5.164 (2)
b (Å)	14.790 (3)	14.796 (8)
c (Å)	7.134 (2)	7.108 (5)
β (°)	106.14 (4)	105.86 (3)
Space group	$P2_1$	$P2_1$
T (K)	122 (0.5)	122 (2)
λ (Å)	0.7107	0.8308
$(\sin\theta)/\lambda_{max}$ (Å^{-1})	1.153	0.774
Measured reflections	8424	2086
(hkl regions)	$\pm H \pm K \pm L$	$\pm H \pm K + \pm L$
Unique reflections	3807	1472
R_{int} (±)	0.014	0.047
Absorption corrections	No	Yes
Number of variables	145	271
wR (F)*	0.044	0.031
wR (F^2)†	0.089	0.062
μ (cm^{-1})	0.846	1.4
Extinction correction	No	Yes
Mosiac spread	—	221 (15) in arc
Extinction factor $y = F_o^2/F_{corr}^2$ less than 0.9	—	y_{120},0.88; y_{101},0.76; y_{021},0.88

* $wR(F) = [(\sum_w |F_o - kF_c|^2)/(\sum_w F_o^2)]^{1/2}$.
† $wR(F^2) = [(\sum_w |F_o^2 - k^2F_c^2|^2)/(\sum_w F_o^4)]^{1/2}$.

During the data collection five standard reflections, $26\bar{2}$, $24\bar{2}$, $23\bar{2}$, $21\bar{4}$, $14\bar{2}$, were measured every 2 h. Data reduction and error analysis were carried out using the programs of Blessing (1989, and reference therein). Reflection integration limits were taken from a Lorentzian model for peak-width variations. A polynomial fit to the smooth decline of *ca* 0.03% in the standard reflection intensities over the 3 weeks of X-ray exposure was used to scale the data. Absorption and beam-inhomogeneity corrections were not necessary. No $\sigma(I)/I$ rejection criteria were applied for the X-ray data. Table 1 summarizes the physical parameters for the two experiments.*

The crystal used in the neutron diffraction measurements was grown by slow evaporation of a solution of NPP in chloroform cyclohexane, and the dimensions were *ca* 7.5 × 7.0 × 1.7 mm. It was quenched in liquid nitrogen to decrease extinction and enclosed in a cylindrical airtight aluminium capsule with a wall thickness of 0.02 mm. The neutron diffraction experiment was performed on the 5C2 four-circle diffractometer installed at the ORPHEE reactor (Laboratoire Leon Brillouin CEN Saclay) using a wavelength of 0.8308 Å. The sample was mounted on a closed-cycle refrigerator and held at 122 K (±2) during the data collection. Integrated reflection intensities were determined from ω scans by profile analysis. The effective linear absorption coefficient $\mu = 1.4$ cm^{-1} was measured by the attenuation of a narrow neutron beam passing through an NPP crystal platelet of known thickness. Cell parameters were determined from refinement using centred angular high positions of 20 reflections. Measurements covered parts of four octants with $-8 < h < 8$, $-22 < k < 22$, $-10 < l < 10$ and $(\sin\theta/\lambda) < 0.8$ Å^{-1}. A total of 2086 reflections were recorded, giving 1472 independent reflections.

* Lists of structure factors and electron-density parameters have been deposited with the IUCr (Reference: PA0296). Copies may be obtained through The Managing Editor, International Union of Crystallography, 5 Abbey Square, Chester CH1 2HU, England.

Neutron and spherical X-ray refinements

The neutron data were corrected for absorption by the Gaussian grid integration method (Coppens, Leiserowitz & Rabinovich, 1965). The position and thermal parameters from an X-ray study at room temperature of Zyss, Nicoud & Coquillay (1984) were used as the starting set in a least-squares minimization of $\sum_w (F_o^2 - k^2F_c^2)^2$. Each reflection was assigned a weight w, inversely proportional to the estimated variance of the observation $w^{-1} = \sigma_c^2(F_o)^2 + (kF_o^2)^2 = \sigma^2(F_o)^2$, where $\sigma_c(F_o)^2$ is based on counting statistics and $k = 0.007$ in the final cycles of refinement. The neutron scattering lengths (in fm) used in the calculations were $b_C = 6.548$, $b_N = 9.40$, $b_O = 5.75$ and $b_H = -3.723$. There was no parameter shift by more than 10% of the standard deviation in the last cycle refinement. The standard deviation of an observation of unit weight was

$$S = \left[\sum_w (F_o^2 - F_c^2)^2/(m-n)\right]^{1/2} = 1.801.$$

The 89 coordinates and 180 anisotropic factors of the atoms, the scale factor and an isotropic secondary parameter for a type I crystal with a Lorentzian distribution of mosaicity were refined to converge to data with $I > 3\sigma(I)$ (1002 reflections) using the program *Linex* (Becker & Coppens, 1974). The resulting atomic parameters are reported in Tables 2 and 3 along with the parameters derived from high-order (HO) refinements [reflections above $(\sin\theta)/\lambda > 0.80$ Å^{-1}] and a full data X-ray refinement. The X-ray scattering factors for C, N and O atoms were taken from the *International Tables for X-ray Crystallography* (1974, Vol. IV), while the bonded H-atom scattering curve of Stewart, Davidson & Simpson (1965) was used for hydrogen.

The positions from HO full data and neutron refinements are very similar, however, for N and O atoms the HO results are closer to the neutron values than the full data coordinates. The full data X-ray results depend on correlations between position parameters and charge density in the bonds.

The X-ray thermal parameters derived from HO in this experiment are smaller than those obtained by neutron scattering. This divergence can typically be attributed to differences in measurement temperatures. A detailed analysis of the vibrational parameters is reported in Table

Table 2. *Fractional atomic coordinates from HO* (I), *neutron* (II) *and full data* (III) *refinements*

		x	y	z
C(1)	I	0.5192 (3)	0.0455	0.4392 (2)
	II	0.5190 (7)	0.0455	0.4387 (7)
	III	0.5193 (2)	0.0455	0.4395 (2)
C(2)	I	0.5356 (3)	0.1393 (1)	0.4566 (2)
	II	0.5365 (7)	0.1388 (4)	0.4553 (7)
	III	0.5356 (3)	0.1393 (1)	0.4559 (2)
C(3)	I	0.6654 (3)	0.1878 (1)	0.3444 (2)
	II	0.6648 (7)	0.1881 (5)	0.3440 (6)
	III	0.6657 (3)	0.1876 (1)	0.3442 (2)
C(4)	I	0.7800 (3)	0.1436 (3)	0.2098 (2)
	II	0.7806 (7)	0.1436 (3)	0.2102 (6)
	III	0.7801 (2)	0.1435 (1)	0.2098 (2)
C(5)	I	0.7637 (3)	0.0479 (1)	0.1976 (2)
	II	0.7632 (7)	0.0486 (4)	0.1981 (6)
	III	0.7636 (3)	0.0479 (1)	0.1975 (2)
C(6)	I	0.6342 (3)	−0.0003 (1)	0.3109 (2)
	II	0.6356 (6)	−0.0004 (5)	0.3114 (6)
	III	0.6347 (3)	−0.0001 (1)	0.3108 (2)
C(7)	I	0.8744 (2)	0.2892 (1)	0.0655 (2)
	II	0.8729 (6)	0.2892 (4)	0.0647 (6)
	III	0.8742 (2)	0.2895 (1)	0.0656 (2)
C(8)	I	0.9034 (3)	0.3012 (1)	−0.1408 (2)
	II	0.9030 (6)	0.3007 (4)	−0.1401 (6)
	III	0.9028 (3)	0.3012 (1)	−0.1410 (2)
C(9)	I	1.0971 (3)	0.2253 (1)	−0.1560 (2)
	II	1.0946 (7)	0.2258 (5)	−0.1587 (7)
	III	1.0975 (3)	0.2255 (1)	−0.1578 (2)
C(10)	I	1.0091 (3)	0.1467 (1)	−0.0516 (2)
	II	1.0070 (7)	0.1472 (4)	−0.0518 (7)
	III	1.0093 (3)	0.1468 (1)	−0.0518 (2)
C(11)	I	1.0927 (3)	0.3409 (1)	0.2164 (2)
	II	1.0903 (6)	0.3404 (4)	0.2160 (6)
	III	1.0927 (3)	0.3407 (1)	0.2166 (2)
N(1)	I	0.3841 (3)	−0.0040 (1)	0.5572 (2)
	II	0.3851 (5)	−0.0045 (4)	0.5570 (5)
	III	0.3842 (2)	−0.0037 (1)	0.5572 (2)
N(2)	I	0.9000 (3)	0.1910 (1)	0.0944 (2)
	II	0.8986 (4)	0.1912 (4)	0.0949 (4)
	III	0.8996 (2)	0.1910 (1)	0.0943 (2)
O(1)	I	0.3483 (3)	−0.0857 (1)	0.5314 (2)
	II	0.3515 (9)	−0.0857 (5)	0.5319 (8)
	III	0.3489 (2)	−0.0859 (1)	0.5315 (1)
O(2)	I	0.3047 (4)	0.0378 (1)	0.6812 (3)
	II	0.3042 (10)	0.0376 (5)	0.6777 (11)
	III	0.3041 (2)	0.0380 (1)	0.6811 (2)
O(3)	I	1.0708 (3)	0.4349 (1)	0.1821 (2)
	II	1.0696 (8)	0.4346 (5)	0.1830 (8)
	III	1.0701 (1)	0.4351 (1)	0.1816 (1)
HC(2)	II	0.4457 (15)	0.1726 (9)	0.5573 (15)
HC(3)	II	0.6798 (17)	0.2597 (7)	0.3611 (15)
HC(5)	II	0.8481 (18)	0.0126 (9)	0.0935 (19)
HC(6)	II	0.6233 (19)	−0.0727 (8)	0.3051 (17)
HC(7)	II	0.6748 (12)	0.3121 (7)	0.0754 (12)
HC(8)	II	0.7109 (14)	0.2915 (8)	−0.2462 (13)
H'C(8)	II	0.9720 (18)	0.3672 (8)	−0.1649 (16)
HC(9)	II	1.3016 (13)	0.2444 (9)	−0.0851 (15)
H'C(9)	II	1.0872 (17)	0.2068 (9)	−0.3125 (16)
HC(10)	II	1.1756 (13)	0.1011 (8)	0.0172 (15)
H'C(10)	II	0.8513 (14)	0.1057 (8)	−0.1509 (13)
HC(11)	*II*	*1.2883 (12)*	*0.3189 (7)*	*0.2059 (15)*
H'C(11)	II	1.0797 (16)	0.3264 (8)	0.3684 (14)
HO(3)	II	0.9243 (15)	0.4580 (8)	0.2282 (16)

Table 3. *Thermal parameters* ($Å^2 \times 10^4$) *from HO* (I), *neutron* (II) *and full data* (III) *refinements*

		U_{11}	U_{22}	U_{33}	U_{12}	U_{13}	U_{23}
C(1)	I	168 (4)	97 (3)	141 (4)	−8 (3)	66 (3)	2 (2)
	II	209 (12)	102 (17)	178 (21)	−27 (14)	78 (13)	6 (16)
	III	150 (5)	112 (4)	145 (5)	−14 (4)	61 (4)	12 (4)
C(2)	I	166 (4)	100 (3)	156 (4)	−6 (3)	80 (3)	−4 (3)
	II	202 (14)	116 (18)	183 (22)	−14 (14)	103 (13)	−7 (15)
	III	166 (6)	111 (4)	161 (5)	−11 (4)	72 (4)	−11 (4)
C(3)	I	162 (4)	85 (3)	158 (4)	1 (3)	72 (3)	−6 (2)
	II	203 (13)	133 (19)	183 (20)	8 (16)	107 (13)	−15 (16)
	III	159 (5)	86 (4)	156 (5)	6 (4)	61 (4)	−6 (4)
C(4)	I	130 (4)	83 (3)	134 (3)	5 (2)	49 (3)	32 (2)
	II	170 (12)	77 (15)	106 (19)	34 (13)	44 (11)	−8 (14)
	III	123 (5)	96 (4)	138 (5)	1 (4)	47 (4)	6 (3)
C(5)	I	197 (5)	82 (3)	165 (4)	8 (3)	92 (4)	−4 (3)
	II	227 (14)	112 (20)	276 (25)	−11 (16)	141 (15)	−29 (18)
	III	186 (5)	95 (4)	170 (5)	13 (4)	82 (4)	−2 (4)
C(6)	I	203 (5)	87 (3)	180 (4)	−2 (3)	91 (4)	1 (3)
	II	233 (14)	95 (17)	209 (23)	−10 (16)	106 (14)	−19 (16)
	III	199 (6)	89 (4)	182 (5)	−1 (4)	85 (4)	0 (4)
C(7)	I	127 (3)	91 (2)	147 (4)	1 (2)	49 (3)	10 (2)
	II	144 (12)	135 (19)	192 (19)	4 (14)	49 (11)	26 (17)
	III	139 (5)	88 (4)	160 (5)	−0 (4)	53 (4)	16 (3)
C(8)	I	208 (5)	135 (3)	145 (4)	−15 (3)	48 (3)	18 (3)
	II	270 (15)	152 (19)	149 (18)	−9 (16)	40 (13)	85 (16)
	III	213 (6)	137 (5)	149 (5)	−12 (4)	58 (4)	16 (4)
C(9)	I	198 (5)	154 (3)	171 (4)	−23 (3)	92 (4)	−8 (3)
	II	248 (14)	199 (21)	186 (23)	−42 (17)	137 (14)	−33 (17)
	III	198 (6)	166 (5)	173 (5)	−20 (4)	94 (4)	−2 (4)
C(10)	I	173 (4)	119 (3)	162 (4)	6 (3)	80 (3)	−8 (3)
	II	161 (12)	155 (19)	182 (22)	−15 (14)	89 (11)	−44 (16)
	III	186 (5)	125 (5)	167 (5)	6 (4)	94 (4)	−18 (4)
C(11)	I	151 (4)	103 (3)	173 (4)	−5 (3)	46 (3)	−13 (2)
	II	168 (12)	108 (17)	168 (19)	6 (12)	56 (11)	−2 (15)
	III	157 (5)	96 (5)	181 (5)	−1 (4)	49 (4)	−11 (4)
N(1)	I	172 (4)	122 (3)	168 (4)	−23 (3)	80 (3)	9 (3)
	II	232 (9)	140 (13)	194 (15)	−35 (11)	110 (9)	18 (12)
	III	164 (5)	130 (4)	169 (4)	−21 (4)	70 (4)	16 (4)
N(2)	I	167 (4)	82 (2)	159 (4)	−3 (2)	82 (3)	−1 (2)
	II	199 (1)	92 (12)	178 (14)	−20 (10)	106 (9)	−25 (12)
	III	176 (5)	74 (4)	160 (4)	−3 (3)	88 (4)	−9 (3)
O(1)	I	250 (5)	113 (2)	212 (4)	−49 (3)	91 (4)	8 (2)
	II	327 (18)	122 (20)	237 (25)	−94 (19)	109 (16)	−10 (20)
	III	250 (5)	117 (4)	215 (4)	−50 (3)	89 (4)	9 (3)
O(2)	I	358 (7)	165 (3)	295 (6)	−39 (4)	238 (6)	−25 (3)
	II	476 (25)	199 (25)	424 (38)	−88 (25)	330 (25)	27 (26)
	III	347 (6)	177 (4)	290 (5)	−28 (4)	229 (5)	−17 (4)
O(3)	I	209 (4)	93 (2)	238 (4)	−16 (2)	118 (3)	−19 (2)
	II	241 (16)	100 (19)	290 (29)	2 (15)	126 (15)	1 (20)
	III	227 (4)	89 (3)	250 (4)	−22 (3)	128 (4)	−23 (3)

5. Average U_{ii} for the HO X-ray and neutron refinements have been calculated for all non-H atoms and for separate groups of atoms, using the ratios $r_{ii} = [\sum U_{ii}(\mathrm{N})]/[\sum U_{ii}(\mathrm{HO})]$.

The results show an important difference of temperature: $r_{ii} \sim 1.2$. The resolution of the X-ray data [$(\sin\theta)/\lambda = 0.75$ or $0.80\ Å^{-1}$] does not appear to influence the result, and the r_{ii} values in group 4 (*cf.* Table 5) with lone-pair atoms are significantly different from the others. The discrepancy of *ca* 20% could imply a 24 K difference between temperatures of both experiments, which seems unreasonable in view of the precautions which were taken. A number of factors indicate that the discrepancies observed between U_{ij} of the two experiments should be related to the quality of the crystal used in the neutron experiment. In particular, the standard deviations in the neutron refinement were large, some anomalies in U_{ii} of the C(4), C(10) and C(11) atoms were observed (*cf.* Table 3), and difficulties were encountered in the refinement to 90° of the γ-angle of the cell. However, we were unable to detect the crystal twin described by Andreazza *et al.* (1992).

Our results confirmed the structure proposed by Zyss *et al.* [1984 (*cf.* Fig. 1)]. The hydrogen bond O(3)—HO(3)···O(2) connects the hydroxyl group with the nitro group of the upper-adjacent molecule and the distance O(3)—O(2) (2.84 instead of 2.86 Å) corresponds to a bonding of intermediate strength (*cf.* Fig. 2). A particularly striking feature of the packing is the proximity of the molecular plane to the (101) crystallographic plane: the calculated angle from the (101)

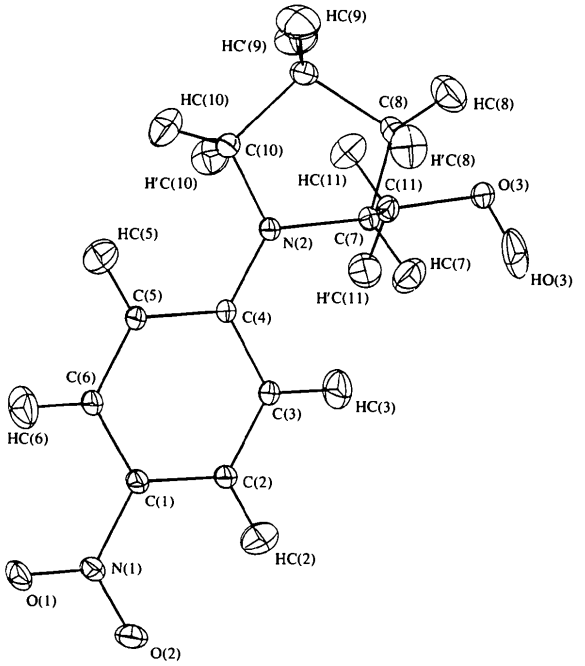

Fig. 1. *ORTEP* (Johnson, 1965) diagram of the NPP molecule. Debye–Waller factors have been calculated from TLS + φ + group tensors of the internal vibrations. Thermal ellipsoids are shown for the 30% probability level.

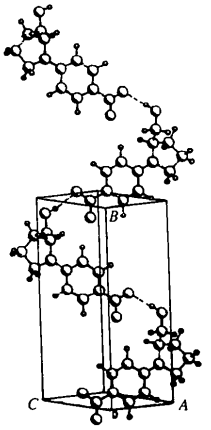

Fig. 2. Molecular packing in the NPP crystal. The hydrogen bond connects one O atom of the nitro group of one molecule to the alcohol group of the next molecule.

Table 4. *Bond lengths* (Å) *and angles* (°) *obtained from X-ray and neutron refinements*

	Length (HO)	Length (N)		Length (HO)	Length (N)
C(1)—C(2)	1.395 (2)	1.386 (5)	C(1)—C(6)	1.396 (2)	1.393 (6)
C(1)—N(1)	1.434 (2)	1.432 (5)	C(2)—C(3)	1.379 (2)	1.372 (6)
C(3)—C(4)	1.419 (2)	1.416 (6)	C(4)—C(5)	1.419 (1)	1.411 (8)
C(4)—N(2)	1.355 (2)	1.345 (5)	C(5)—C(6)	1.380 (2)	1.377 (6)
C(7)—C(8)	1.530 (2)	1.516 (6)	C(7)—C(11)	1.532 (2)	1.527 (6)
C(7)—N(2)	1.470 (2)	1.467 (8)	C(8)—C(9)	1.526 (2)	1.515 (7)
C(9)—C(10)	1.516 (2)	1.524 (7)	C(10)—N(2)	1.469 (2)	1.464 (5)
C(11)—O(3)	1.413 (2)	1.413 (8)	N(1)—O(1)	1.231 (2)	1.221 (8)
N(1)—O(2)	1.239 (2)	1.223 (7)	C(2)—HC(2)		1.09 (1)
C(3)—HC(3)		1.07 (1)	C(5)—HC(5)		1.10 (1)
C(6)—HC(6)		1.07 (1)	C(7)—HC(7)		1.10 (1)
C(8)—HC(8)		1.08 (1)	C(8)—H'C(8)		1.08 (1)
C(9)—HC(9)		1.09 (1)	C(9)—H'C(9)		1.12 (1)
C(10)—HC(10)		1.11 (1)	C(10)—H'C(10)		1.10 (1)
C(11)—HC(11)		1.09 (1)	C(11)—H'C(11)		1.12 (1)
O(3)—HO(3)		0.96 (1)			

	X-ray	Neutron
C(2)—C(1)—C(6)	120.6 (1)	120.7 (4)
C(11)—C(7)—N(2)	112.1 (1)	111.6 (4)
C(2)—C(1)—N(1)	119.0 (3)	119.7 (3)
C(7)—C(8)—C(9)	103.3 (1)	104.0 (4)
C(6)—C(1)—N(1)	120.4 (1)	119.6 (3)
C(8)—C(9)—C(10)	103.3 (1)	103.0 (4)
C(1)—C(2)—C(3)	119.7 (1)	120.7 (4)
C(9)—C(10)—N(2)	103.7 (1)	103.8 (4)
C(2)—C(3)—C(4)	120.8 (1)	120.1 (4)
C(7)—C(11)—O(3)	110.9 (1)	111.4 (4)
C(3)—C(4)—C(5)	118.2 (1)	118.2 (4)
C(1)—N(1)—O(1)	119.5 (1)	119.7 (4)
C(3)—C(4)—N(2)	121.1 (1)	120.7 (4)
C(1)—N(1)—O(2)	118.6 (1)	117.5 (4)
C(5)—C(4)—N(2)	120.6 (1)	121.1 (4)
O(1)—N(1)—O(2)	122.3 (2)	122.9 (5)
C(5)—C(5)—C(6)	120.6 (1)	121.4 (4)
C(4)—N(2)—C(7)	124.1 (1)	124.6 (4)
C(1)—C(6)—C(5)	119.9 (1)	119.0 (4)
C(4)—N(2)—C(10)	121.9 (1)	121.7 (4)
C(8)—C(7)—C(11)	111.7 (1)	111.8 (4)
C(7)—N(2)—C(10)	112.3 (1)	111.9 (3)
C(8)—C(7)—N(2)	102.5 (1)	102.9 (4)
C(1)—C(2)—HC(2)		119.0 (7)
C(3)—C(2)—HC(2)		120.3 (7)
C(8)—C(9)—HC(9)		110.6 (7)
C(8)—C(9)—H'C(9)		114.8 (7)
C(10)—C(9)—HC(9)		109.8 (7)
C(10)—C(9)—H'C(9)		111.1 (6)
HC(9)—C(9)—H'C(9)		107.4 (9)
C(2)—C(3)—HC(3)		119.6 (7)
C(4)—C(3)—HC(3)		120.5 (7)
C(4)—C(5)—HC(5)		199.6 (8)
C(6)—C(5)—HC(5)		119.0 (8)
C(9)—C(10)—HC(10)		112.7 (6)
C(9)—C(10)—H'C(10)		111.8 (6)
N(2)—C(10)—HC(10)		111.4 (6)
		Neutron
N(2)—C(10)—H'C(10)		110.4 (6)
HC(10)—C(10)—H'C(10)		106.8 (8)
C(5)—C(6)—HC(6)		122.2 (7)
C(1)—C(6)—HC(6)		118.8 (7)
N(2)—C(7)—HC(7)		110.0 (6)
C(8)—C(7)—HC(7)		111.9 (6)
C(11)—C(7)—HC(7)		108.5 (6)
C(7)—C(8)—HC(8)		110.0 (6)
C(7)—C(8)—H'C(8)		112.6 (7)
C(9)—C(8)—HC(8)		110.2 (6)
C(9)—C(8)—H'C(8)		113.6 (7)
HC(8)—C(8)—H'C(8)		106.4 (9)
C(7)—C(11)—HC(11)		109.3 (6)
C(7)—C(11)—H'C(11)		111.6 (6)
O(3)—C(11)—HC(11)		107.9 (7)
HC(11)—C(11)—H'C(11)		107.7 (8)
O(3)—C(11)—H'C(11)		108.8 (7)
C(11)—O(3)—HO(3)		109.3 (8)

Table 5. *Values obtained for* $\bar{U}_{ii}$ ($Å^2 \times 10^4$) *from HO and neutron refinements, and for the ratios* $r_{ii} = [\sum \bar{U}_{ii}(N)]/[\sum \bar{U}_{ii}(HO)]$ *for all atoms and for separate groups of atoms*

Group	Atoms	HO	$\bar{U}_{11}$(HO)	$\bar{U}_{22}$(HO)	$\bar{U}_{33}$(HO)	$\bar{U}_{11}$(N)	$\bar{U}_{22}$(N)	$\bar{U}_{33}$(N)	HO	r_{11}	r_{22}	r_{33}
1	All	≥ 0.80	189	107	175	231	127	208	≥ 0.80	1.22	1.19	1.19
2	Phenyl ring	≥ 0.80	171	89	156	207	106	190	≥ 0.80	1.21	1.19	1.22
3	Pyrrolidine ring	≥ 0.80	171	114	160	198	139	176	≥ 0.80	1.16	1.22	1.10
4	Nitro group	≥ 0.80	260	133	225	345	153	285	≥ 0.80	1.32	1.15	1.27

Table 6. *Differences in MSDA values* [$10^4 \times \Delta$(MSDA) $Å^2$], *obtained from HO refinement for pairs of atoms in the NPP molecule; underlined values correspond to chemical bonds*

	O(3)	O(2)	O(1)	N(2)	N(1)	C(11)	C(10)	C(9)	C(8)	C(7)	C(6)	C(5)	C(4)	C(3)	C(2)
C(1)	9	1	−5	−4	−6	26	13	13	21	−1	7	1	0	1	2
C(2)	10	19	−10	−1	−2	32	9	11	21	1	−1	−7	4	9	
C(3)	6	9	−7	−10	−8	21	−3	0	8	−8	3	−6	0		
C(4)	6	6	7	−5	−6	16	4	10	15	1	5	−1			
C(5)	0	−2	14	−12	−8	7	11	12	12	−2	2				
C(6)	4	−14	13	−12	−13	15	8	9	12	−4					
C(7)	4	19	4	−5	−3	0	4	12	6						
C(8)	1	−2	−11	−6	−24	8	−8	−12							
C(9)	−30	−2	−2	−11	−18	−6	−2								
C(10)	−20	−6	4	−4	−19	−12									
C(11)	−4	−15	−30	−4	−36										
N(1)	15	−9	−13	2											
N(2)	6	13	15												
O(1)	15	−6													
O(2)	11														

plane is 5.24° instead of 11° at room temperature. The angle between the charge transfer axis N(1)—N(2) and the binary axis is 58.9° (Zyss & Oudar, 1982), which is highly favourable to non-linear interactions in the compound. A comparison of distances and angles obtained from the X-ray and neutron measurements is listed in Table 4. The C—H and O—H distances from neutron data refinement are also reported.

Rigid-bond and rigid-molecule tests

According to Hirshfeld (1976), the mean-square displacement amplitudes (MSDA) for two atoms in a pair of bonded non-H atoms in a typical organic molecule should be almost identical along the bond direction, although they may differ widely along other orientations. For well refined structures based on good data sets, differences in MSDA for rigid bonds are usually smaller than 10×10^{-4} $Å^2$. Differences in MSDA values [$10^4 \times \Delta$(MSDA) $Å^2$] obtained in this work from HO refinements are listed in Table 6. The average MSDA obtained for bond pairs is 4.84×10^{-4} $Å^2$, and thus the displacement parameters correspond to typical values for rigid bonds. However, columns 1, 2, 3 and 6 which list the projections on virtual bonds provide some clues about the internal motions of the fragments within the molecule. In column 6, the MSDA of C(11) are all large except for nearest neighbours O(3) and C(7); in columns 2 and 6 the large values between O(2), O(1) and C(2), C(6) indicate that there is considerable motion between the nitro group and the pyridine ring.

Rigid-body model

A least-squares analysis of the rigid-body motion of the molecule was carried out according to the model of Schomaker & Trueblood (1968). Some Δ(MSDA) values in Table 6 suggest that the molecule is not entirely rigid and that low frequency soft modes of intermolecular vibration contribute significantly to the observed mean-square displacements (Rosenfield, Trueblood & Dunitz, 1978). The mean-square atomic displacements were modelled by fitting molecular T, L and S plus correlated Φ_i tensors to the atomic U tensors. T, L and S model the external lattice vibrations of the whole molecule, Φ_i model low-frequency large-amplitude internal molecular vibrations, as librations of rigid groups of atoms within the flexible molecule (Dunitz, Schomaker & Trueblood, 1988; Dunitz, Maverick & Trueblood, 1988). Table 7 summarizes some results which show that at 122 K the lattice vibrations are damped such that the internal libration contribution to the total mean-square atomic displacements is as important or larger than the contribution from the external librations. A few models were used to describe the internal librations. The best results were obtained for two librating rigid groups around the C(4)—N(2) and C(1)—N(1) bonds. In the inertial reference frame, the

Table 7. *Principal mean-square amplitudes and torsional force constants from the fit of molecular TLS + Φ_i to the atomic U_{jk}*

	Rigid molecule	Flexible molecule	Whole translations $\langle t^2 \rangle$ (Å^2)	Molecule librations $\langle \lambda^2 \rangle$ (deg^2)
R	0.127	0.075	t_{11} 0.00086 (13)	L_{11} 2.82 (42)
r.m.s. of Δ	0.0014	0.0009	t_{22} 0.00041 (19)	L_{22} 1.33 (62)
n	96	96	t_{33} 0.00044 (8)	L_{33} 1.44 (27)
m	20	32		
Librating Group	Libration Axis	Torsion Angle	$\langle \varphi^2 + 2\varphi \rangle$ (deg^2)	Force constants (J mol^{-1} deg^2)
C(7), C(8), C(9), C(11)	C(4)—N(2)	φ_1	1.4	1750 (1000)
O(2), O(1)	C(1)—N(1)	φ_2	36.8	29 (10)

Direction cosines			Inertial moments	L (deg^2)		
x	y	z				
−0.589	−0.638	0.494	324	3.61	−0.34	−0.93
0.293	−0.739	−0.605	1920	0.82	−0.23	
0.753	−0.211	0.622	2201	1.18		

L refers to the inertial axes of the molecule.

off-diagonal matrix elements are somewhat small and $L_{11} = 3.6$ deg^2 shows that the overall libration motion occurs around the axis with the smallest inertial moment which corresponds, for NPP, to the charge-transfer axis of the molecule.

The TLS + Φ_i analyses were carried out using the *THMA*11 program (Trueblood, 1990), which includes a six-parameter model for the physical correlations between each internal torsional mode and the external lattice mode.

Vibration analysis of the H atoms

The R-factors resulting from least-squares refinements (HO spherical or multipolar) are higher when using the neutron Debye–Waller factors than those deduced from X-ray refinements. Rescaling the thermal parameters derived from neutron data using the ratio given in Table 5 is not sufficient to reproduce the quality of the results obtained from parameters calculated from X-ray data alone. However, the position parameters deduced from X-rays and neutron measurements can be interchanged with no modification to the results.

For the H atoms, the position parameters were taken from the neutron refinement data and the thermal parameters were approximated by a rigid molecular motion and internal C—H vibrations. The total vibration tensor for each H atom is then obtained by the sum of these two contributions (Baert, Schweiss, Heger & More, 1988). For the H atoms of the phenyl ring, the frequencies led to estimated mean-square displacements of 0.0056, 0.014 and 0.025 Å^2 for bond stretching, in-plane bending and out-of-plane bending, respectively, while 0.0057, 0.015 and 0.022 Å^2 were used for the H atoms of the L-prolinol ring. For the H atoms of the hydroxyl group involved in hydrogen bonding with a neighbouring molecule, 0.005, 0.025 and 0.012 Å^2 were used. The torsional librations around C(7)—C(11) and C(11)—O(3) bonds were neglected. A contribution from these modes was already implicit in the calculation of the T and L tensors. The Φ_i libration around C(4)—N(2) bonds was included, as described by Baert *et al.* (1988). The thermal parameters of the H atoms thus calculated are listed in Table 8 along with those derived from the refinement of neutron data after rescaling by an isotropic coefficient of 1.20. Fig. 1 is an *ORTEP* (Johnson, 1965) diagram of the NPP molecule, ellipsoids of the H atoms represent their thermal motions which have been discussed above.

Table 8. *Debye–Waller factors of the* H *atoms* (Å$^2 \times 10^2$) *from TLS + Φ + internal vibrations* (I) *and neutron rescaled values* (II)

		U_{11}	U_{22}	U_{33}	U_{12}	U_{13}	U_{23}
HC(2)	I	393	335	320	51	195	−59
	II	355 (40)	358 (61)	273 (56)	43 (44)	209 (39)	−24 (55)
HC(3)	I	381	146	363	−8	92	−25
	II	349 (37)	106 (41)	302 (51)	−8 (32)	175 (35)	19 (37)
HC(5)	I	425	297	294	73	172	−48
	II	446 (43)	225 (45)	444 (79)	39 (46)	295 (47)	−315 (52)
HC(6)	I	445	143	368	−15	86	−4
	II	462 (47)	143 (40)	350 (61)	−60 (44)	209 (41)	−1 (43)
HC(7)	I	226	245	389	46	130	7
	II	203 (24)	227 (41)	249 (47)	48 (30)	87 (25)	81 (39)
HC(8)	I	322	319	275	−16	−74	22
	II	321 (48)	327 (45)	195 (62)	−72 (44)	119 (41)	157 (49)
H′C(8)	I	411	243	309	−74	130	24
	II	480 (32)	247 (56)	323 (46)	−4 (41)	−7 (27)	42 (40)
HC(9)	I	259	382	359	−48	131	−87
	II	234 (42)	310 (55)	385 (48)	−43 (43)	100 (35)	−419 (54)
H′C(9)	I	473	390	233	−49	170	−78
	II	488 (30)	296 (55)	205 (61)	−45 (39)	89 (31)	9 (37)
HC(10)	I	312	276	288	−40	70	−77
	II	272 (31)	308 (57)	435 (61)	212 (40)	71 (32)	−80 (53)
H′C(10)	I	318	267	313	99	78	−33
	II	345 (32)	313 (58)	210 (43)	−85 (39)	125 (30)	184 (45)
HC(11)	I	230	298	331	40	90	−47
	II	150 (23)	206 (41)	525 (65)	22 (30)	77 (26)	11 (48)
H′C(11)	I	406	242	219	40	129	54
	II	503 (46)	302 (58)	180 (58)	−32 (48)	83 (38)	−28 (43)
HO(3)	I	490	200	302	30	188	−27
	II	288 (35)	229 (44)	500 (76)	62 (40)	210 (39)	−3 (54)

Kappa and multipole refinements

All refinements minimized the function $\sum w(|F_o|^2 - k^2|F_c|^2)^2$, where $w = 1/[\sigma^2(F^2)]$ and $\sigma^2(F^2) = \sigma^2_{\text{counting}}(F^2) + (p|F|^2)^2$. The instrumental instability factor p was estimated from errors in the time-dependent scaling polynomials and the fluctuations of the standard reflections, giving a value of $p = 0.010$. Anisotropic temperature factors for the H atoms were fixed at their values determined above, and the positions derived from neutron data refinements were used. The y-coordinate of C(1) was fixed to define the origin of the polar space group. Atomic scattering factors for the C, N and O neutral atoms were taken from the *International Tables for X-ray Crysallography* (1974, Vol. IV). The bound-atom form factor for hydrogen was taken from Stewart *et al.* (1965).

The rigid pseudo-atom model of Hansen & Coppens (1978) is commonly used to analyse the charge density distribution. The electron density $\rho(r)$ in the crystal is described by a sum of so-called aspherical pseudo-atoms with nuclear positions r_k

$$\rho(\mathbf{r}) = \sum_k \rho_k(\mathbf{r} - \mathbf{r}_k - \mathbf{u}) * t_k(\mathbf{u}), \qquad (2)$$

where $t_k(\mathbf{u})$ is a Gaussian thermal-displacement distribution and * indicates a convolution product. Each atomic density is described as a series expansion in real spherical harmonic functions (Y_{lm}) up to order four

$$\rho_k(\mathbf{r}) = P_{k,c}\rho_{k,c}(\mathbf{r}) + P_{k,v}\kappa^3\rho_{k,v}(\kappa, r) + \sum_{l=0}^{4} \kappa'^3 R_l(\kappa', r) \sum_{m=-l}^{l} P_{lm} Y_{lm}(\mathbf{r}/|r|). \qquad (3)$$

In (3), ρ_c and ρ_v are spherically averaged Hartree–Fock core and valence densities, with ρ_v normalized to one electron. The Slater-type radical functions $R_l = N_l r^n \exp(-\kappa'\zeta r)$ are modulated by the multipolar spherical harmonic angular functions Y_{lm} and N_l is a normalization factor. The values for parameters $n = n_l$ and ζ were chosen according to rules provided by Hansen & Coppens (1978): $n_l = 2, 2, 3, 4$ and $\zeta_l = 2.8, 4.0, 5.06, 2.0$ (Å^{-1}) for C, O, N, H were used, respectively, for $l = 1, 2, 3, 4$. ζ_l values were free to vary during the refinement. The adjustable variables are the valence-shell contraction–expansion parameters κ and κ' and the population parameters P_v and P_{lm}. The truncation to $l = 4$ corresponds to the multipole expansion at the hexadecapole level for the non-H atoms. To reduce the number of variables, chemical constraints were imposed on the multipole parameters: atoms of similar environment were assumed to have the same deformation. Local symmetry and deformation types are summarized in Table 9. Local pseudo-atom coordinate systems are defined in Fig. 3.

Multipolar refinements provide quantitative results and can thus be used to complement more qualitative $X - X_{HO}$ or $X - X_N$ studies. Since the structures of the quadratic NLO compounds are non-centrosymmetric, the multipolar procedure is essential to evaluate the phases of the structure factors in order to obtain reliable electron density maps and one-electron properties. Recent applications by Souhassou *et al.* (1991) have demonstrated the usefulness and the potential accuracy of the method. Fig. 4 shows the distribution of $2|Fs|\sin(\Delta\varphi)/2$ as a function of $(\sin\theta)/\lambda$ and $|F|$. As expected, due to the highly diffuse distribution of the valence electron, $2|Fs|\sin(\Delta\varphi)/2$ tends to increase with decreasing $(\sin\theta)/\lambda$ [Fig. 4(*a*)]. It is also apparent [Fig. 4(*b*)] that the weak and intermediate reflections have a strong influence.

Two least-squares refinements were carried out; in both procedures, the hydrogen position parameters were

Table 9. *Local site symmetry and deformation types imposed to the atoms of the molecule*

Atoms	Deformation type	Local site symmetry
N(2)	1	*m*
C(2),C(3),C(4),C(6)	2	*m*
C(1),C(4)	3	*m*
N(1)	4	*m*
O(1),O(2)	5	*m*
C(8),C(9),C(10)	6	*m*
C(7)	7	*m*
C(11)	8	*m*
O(3)	9	*m*
HC(2),HC(3),HC(5),HC(6) HC(7),HC(8),H'C(8),HC(9) H'C(9),HC(10),H'C(10) HC(11),H'C(11),HO(3)	10	*mm*

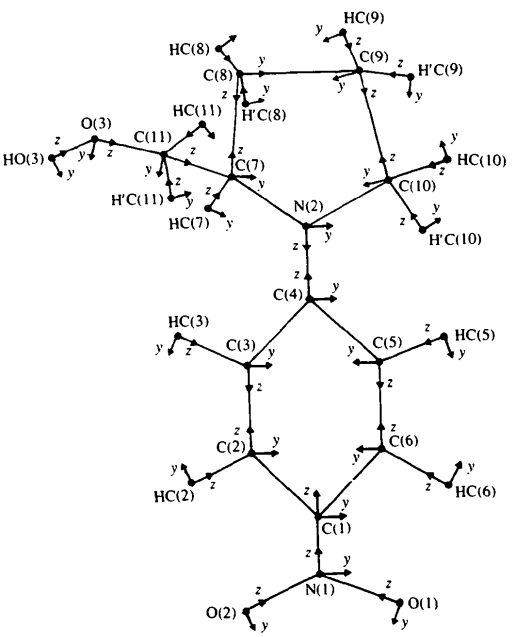

Fig. 3. Labelling of the atoms and definition of local orthogonal reference axes for the atom-centred multipolar functions.

Table 10. *Review of least-squares refinements (X-ray data)*

	Full spherical refinement	HO [$(\sin\theta)/\lambda = 0.80$ Å^{-1}] refinement	Kappa refinement	Multipolar refinement
N_o	3807	1833	3807	3807
N_v	144	144	185	433
$R(F)$	0.042	0.045	0.041	0.026
$wR(F)$	0.044	0.035	0.031	0.012
$R(F^2)$	0.059	0.061	0.049	0.020
$wR(F^2)$	0.089	0.067	0.063	0.023
S	1.95	0.964	2.69	1.02
k	7.288	7.343	7.10	7.24
w'	$[\sigma^2(F_o)]^{-1}$	$[\sigma^2(F_o)]^{-1}$	$[\sigma^2(F_o)]^{-1}$	
w				$[\sigma^2(F_o^2) + 0.01^2F_o^4]^{-1}$

$R(F) = \sum_{hkl}(F_o - k\|F_c\|)/\sum_{hkl}F_o$; $wR(F) = [\sum_{hkl}w'(F_o - k\|F_c\|)^2/\sum_{hkl}w'F_o^2]^{1/2}$; $R(F^2) = \sum_{hkl}[F_o^2 - (k\|F_c\|)^2]/\sum_{hkl}F_o^2$; $wR(F^2) = [\sum_{hkl}w[F_o^2 - (k\|F_c\|)^2]^2/\sum_{hkl}wF_o^4]^{1/2}$; $S = [\sum_{hkl}(F_o^2 - k\|F_c\|^2)2/(N_o - N_v)]^{1/2}$; N_o = number of independent observed reflections; N_v = number of refined parameters; k = scale factor; w,w' = weight coefficients.

kept fixed to the value obtained by the neutron data refinement, and the thermal parameters calculated from the TLS + φ_i tensors and internal contributions were also fixed.

The κ refinement allows the adjustment of the valence-shell population along with the structural parameters of the heavy atoms. Extension and contraction of the valence shell is taken into account by introducing a κ parameter which relates the perturbed valence density

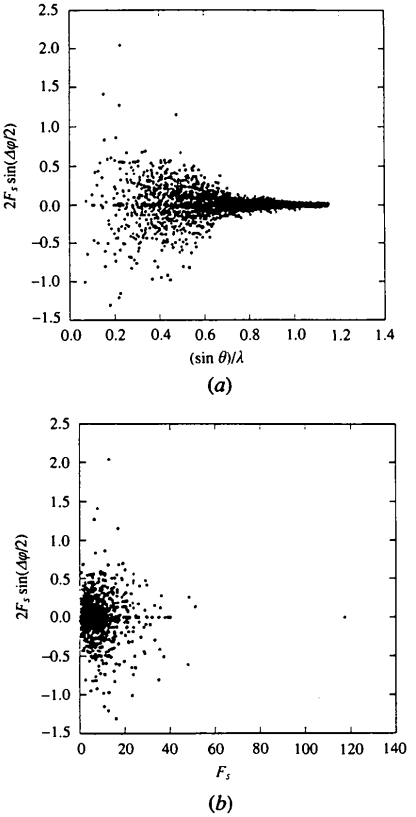

Fig. 4. Distribution of $2F\sin(\Delta\varphi/2)$ (in units of electrons) with (*a*) $(\sin\theta)/\lambda$ and (*b*) $|F|$.

Table 11. *Net atomic charges* (+e) *in NPP*

(*A*) Fuzzy boundaring partitioning of experimental density; (*B*) kappa refinement; (*C*) multipolar refinement.

	A	*B*	*C*
C(1)	−0.07	−0.11 (6)	0.20 (1)
C(2)	−0.02	−0.10 (5)	−0.25 (8)
C(3)	−0.09	−0.47 (6)	−0.31 (8)
C(4)	0.03	0.29 (6)	0.10 (1)
C(5)	−0.18	−0.53 (5)	−0.35 (8)
C(6)	−0.13	−0.24 (5)	−0.39 (9)
C(7)	−0.03	−0.33 (9)	−0.40 (1)
C(8)	−0.08	−0.29 (5)	−0.44 (8)
C(9)	−0.08	−0.46 (5)	−0.45 (7)
C(10)	0.01	−0.12 (5)	−0.51 (6)
C(11)	−0.10	−0.29 (8)	−0.30 (1)
N(1)	0.19	0.51 (7)	0.20 (1)
N(2)	−0.04	−0.19 (7)	0.08 (7)
O(1)	−0.18	−0.43 (5)	−0.27 (6)
O(2)	−0.10	−0.43 (5)	−0.20 (6)
O(3)	−0.19	−0.62 (7)	−0.34 (5)
HC(2)	0.08	0.20 (3)	0.22 (3)
HC(3)	0.08	0.29 (2)	0.23 (3)
HC(5)	0.05	0.31 (3)	0.32 (3)
HC(6)	0.06	0.28 (3)	0.25 (3)
HC(7)	0.12	0.27 (2)	0.31 (3)
HC(8)	0.08	0.31 (2)	0.28 (3)
H′C(8)	0.01	0.18 (3)	0.23 (3)
HC(9)	0.04	0.23 (3)	0.23 (3)
H′C(9)	0.09	0.29 (3)	0.27 (3)
HC(10)	0.06	0.23 (3)	0.27 (3)
H′C(10)	0.09	0.21 (3)	0.28 (3)
HC(11)	0.06	0.29 (3)	0.27 (3)
H′C(11)	0.06	0.22 (3)	0.24 (3)
HO(3)	0.17	0.46 (3)	0.32 (3)

$\rho'_{\rm val}(r)$ to the free atom ground state density $\rho_{\rm val}(r)$

$$\rho'_{\rm val}(r) = P_{\rm val}\kappa^3\rho_{\rm val}(\kappa r), \qquad (4)$$

where $P_{\rm val}$ is the valence shell population.

In the multipole refinements, the expansion was truncated at the hexadecapole ($l = 4$) for C, O and N atoms, and at the dipole level ($l = 1$) for the H atoms. The refinements are summarized in Table 10. A large decrease in the *R*-factors is observed between the spherical (HO, full, kappa) and the multipolar refinements. Experimental pseudo-atom charges (electrons) for the two types of refinements with those from fuzzy

boundaries are reported in Table 11. Electron density maps in the phenyl ring prior and after corrections of the phases (*cf.* Fig. 5) clearly illustrate the phase problem extensively discussed by Souhassou *et al.* (1991). Residual maps (*cf.* Fig. 6) show the model is valid for the study of the NPP molecule.

Direct integration method

Results from multipolar refinements are expressed in terms of density functions with populations determined by least-squares adjustments performed in the scattering space. The integration of the electron distribution can also be performed directly in crystal space without using the model functions. This method is examined here. Properties which depend on the electron distribution can be defined by an operator equation

$$\langle \mathcal{O} \rangle = \int \hat{\mathcal{O}} \rho(r) \mathrm{d}^3 r, \qquad (5)$$

where the integration is performed over the complete crystal or a volume associated with a molecule, an ion or an atom. These properties are usually the molecular dipole, quadrupole and octupole moments. The validity of the results depends on the partition of the real space in atomic or molecular moments. Defining the volume is somewhat arbitrary: it is similar to choosing a set of density basis functions in the multipolar formalism.

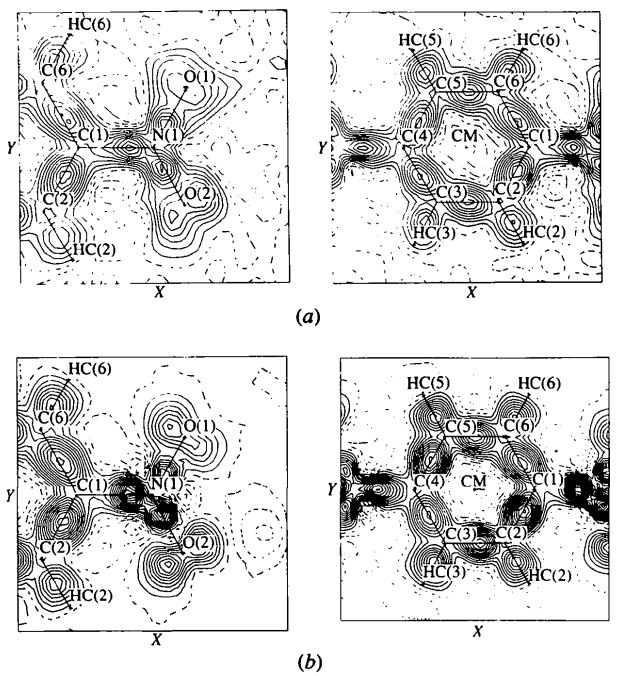

Fig. 5. Multipole deformation density maps calculated in the plane of the nitro group and in the phenyl ring. Contour intervals for 0.05 e Å^{-3}; positive contours are shown as solid lines and negative contours are shown as dashed lines. (*a*) Without phase correction; (*b*) with phases derived from multipolar refinement.

An acceptable volume partition must satisfy a space-filling condition ($\Sigma_i v_i = v$), where v is the cell volume, and furthermore, the unit cell must be neutral ($\Sigma_i q_i = 0$). In this study two methods have been prospected: the discrete boundary scheme (Coppens, 1975) and the 'stockholder concept' proposed by Hirshfeld (1977).

(1) In the discrete boundary partitioning, the boundary surface is defined by the condition

$$[(\mathbf{r} - \mathbf{r}_A) . \hat{r}_{AB}]/R_A = [(\mathbf{r} - \mathbf{r}_B) . - \hat{r}_{AB}]/R_B, \qquad (6)$$

where $\hat{r}_{AB}$ is a unit vector pointing from atom A to atom B, and R_A R_B are the van der Waals radii of atoms A and and B and are free to vary when the molecular moment is investigated.

(2) In the so-called fuzzy boundary or stockholder method, real space is partitioned in overlapping atomic volumes by the use of atomic weighting functions

$$w_i(r) = \sum_{\text{atoms in molecule}} \rho_{\text{sph}} / (\textstyle\sum_{\text{crystal}} \rho_{\text{sph}}). \qquad (7)$$

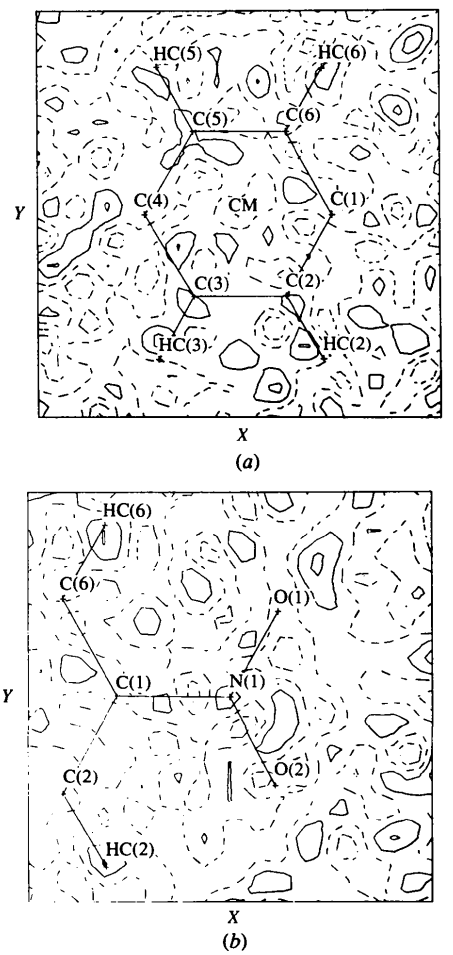

Fig. 6. Residual density, $\Delta\rho(r) = v^{-1} \sum_h (k^{-1}|F_o| - |F_m|) \exp(i\varphi_m) \times (-i2\pi \mathbf{h} . \mathbf{r})$ in the plane of the nitro group, and in the phenyl ring. Contours as in Fig. 5.

Table 12. *Components of the dipolar moment calculated from different methods*

The origin coincides with the centre of mass of the molecule; x is from the nitrogen of the donating group towards the nitrogen of the nitro accepting group, y is in the mean plane perpendicular to x.

	x	y	z	$\|\mu\|$ (Debye)	$\|\beta\|$ (e Å^{-3})
μ (kappa refinement)	−3.45	−0.286	0.47	16.8 (0.6)	
μ (multipolar refinement)	−1.98	0.206	0.111	9.6 (1.4)	
μ (discrete boundary)	−1.55	0.58	0.26	8.1	
μ (fuzzy boundary)	−1.29	0.57	0.26	6.9	
β_{tot}	−42.3	0.39	7.2		42.9
β_{vec}	−39.12	0.14	1.10		39.2

Angles Between	μ^K	μ^M	μ^D	μ^F	β_{tot}	β_{vec}
μ^K	0.0	12.5	25.3	28.8	6.3	10.0
μ^M		0.0	16.1	20.1	9.1	7.3
μ^D			0.0	5.7	19.8	19.7
μ^F				0.0	23.3	25.4
β_{tot}					0.0	8.2
β_{vec}						0.0

The spherical atom densities ρ_{sph} have been calculated from Clementi wavefunctions (Clementi, 1965). Contracted Gaussian wavefunctions have provided similar results. The calculated molecular dipole moments in the crystal using the spherical and the aspherical formalisms are given in Table 12, along with the results of the DB and FB crystal space integration methods.

Given that the molecular volume is defined in different ways, there is reasonable agreement in both magnitude and direction between the different X-ray results, except in the case of the result of the kappa refinement. This last method, as noted above, is inadequate to solve the phase problem. The orientation of the dipolar moments from the four methods range between 6 and 29° and are distributed on either side of the charge transfer N(1)—N(2) axis of the molecule (*cf.* Fig. 7).

Description of quadratic hyperpolarizabilities

Traditionally, the classification of quadratic non-linear molecules is based on a two-level quantum model of the hyperpolarizability β (Oudar, 1977), and on an experimental technique to measure a combination of the tensor coefficients. Although all the 27 components of the β tensor can be computed, only the vector components along the dipole moment direction β_{vec} are sampled experimentally in EFISHG experiments (Kanis, Ratner & Marks, 1992)

$$\beta_{vec}(-2w, w, w) = \sum_{i=1}^{3}(\boldsymbol{\mu}_i \cdot \boldsymbol{\beta}_i)/|\mu|. \qquad (8)$$

In this equation, $\boldsymbol{\mu}$ is the ground-state molecular dipole moment and $\boldsymbol{\beta}_i$ is a component of the so-called vector part of the tensor β with

$$\beta_i = \beta_{iii} + \tfrac{1}{3}\sum_{j\neq i}(\beta_{ijj} + \beta_{jij} + \beta_{jji}), \qquad (9)$$

where the indices i and j represent the molecular Cartesian directions X, Y and Z. More recently, the harmonic light-scattering technique (HLS), initially proposed by Tehrune, Maker & Savage (1965), has been applied to investigate a wide range of molecules. As no poling field is required in this approach (Zyss & Ledoux, 1994), ionic and non-dipolar systems can be measured. This procedure indicates well the limits on the classification of molecules in terms of their non-linear susceptibilities in the absence of information on their ground-state dipole moment in the crystal, on the contribution from octupolar anisotropy and on the angle between β_{vec} and μ. Robinson (1967) has shown that using the Unsöld approximation, the non-linear d_{ijk} susceptibilies can be evaluated from the octupole moment of the charge distribution. The starting point is the fact that π-electrons are delocalized over the volume of the system and thus have to be treated globally. It is the asymmetry in the distribution of these π-electrons which is responsible for the dipole moment and the first-order hyperpolarizabilities β.

Using stationary perturbation theory for states well under any electronic resonance, the non-linear coeffi-

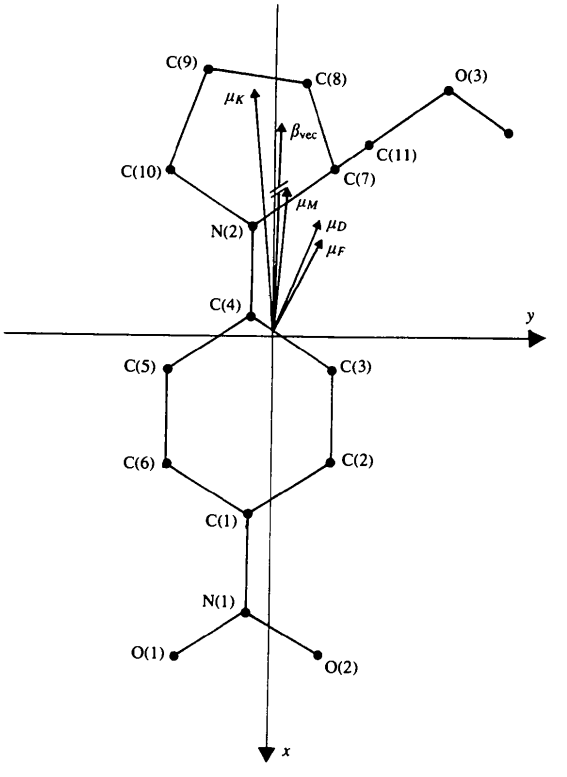

Fig. 7. Dipolar molecular moment calculated by different methods and β_{vec}. The origin is at the centre of mass of the molecule. x is oriented from the nitrogen of the donating group towards the nitrogen of the nitro accepting group, y is directed in the mean molecular plane perpendicular to x.

Table 13. *Values of β from finite field and SOS calculations are compared with the coefficients T_{ijk} of the octupolar moment* (e Å^{-3}) *derived from electron-density study*

x is from the nitrogen of the donating group, towards the nitrogen of the nitro accepting group, y is in the mean molecular plane perpendicular to x (Barzoukas *et al.*, 1987).

β_{ijk}^{2w} 10^{-30}e.s.u	Discrete partition	Diffuse partition	Finite field method	CNDOVSB method $\hbar w = 0$	$\hbar w = 1.17$ e-V
β_{zzz}	−28.70	−23.07	−17.2	−15.49	−29.46
β_{xxy}	−3.21	−3.07	0.15	0.07	0.005
β_{xxz}	4.39	4.08	0.20	−0.12	−0.32
β_{xyy}	−9.24	−8.22	2.30	1.95	3.74
β_{xyz}	0.19	−0.03	−0.1	−0.05	−0.06
β_{xzz}	−4.35	−4.17	0.3	0.03	0.04
β_{yyy}	4.24	3.74	0.3	0.08	0.16
β_{yyz}	0.69	0.79	−0.1	0.05	0.09
β_{yzz}	−0.64	−0.65	0.1	0.01	0.01
β_{zzz}	2.16	2.10	−0.2	−0.01	−0.01

cients d_{ijk} for N molecules in the unit volume can be written as

$$d_{ijk} = (3N\alpha/a_0 e)(T_{ijk}/n), \qquad (10)$$

where $a_0 = h/me^2 = 0.53$ Å, α is the atomic polarizability and n is the number of valence electrons. If $N = 1$, d_{ijk} can be replaced in (10) by β_{ijk}, the molecular hyperpolarizability.

Within a prefactor, T_{ijk} is the octupole moment of the charge distribution. If the electron density in the molecule is ρ then

$$T_{ijk} = \int\int\int \hat{r}_i \hat{r}_j \hat{r}_k \rho(\mathbf{r}) \mathrm{d}^3 r. \qquad (11)$$

Table 13 lists the ten components of β obtained here and those obtained from calculations from finite field and SOS methods (Barzoukas, Josse, Fremeaux & Zyss, 1987; Barzoukas, Josse, Fremeaux, Zyss, Nicoud & Morley, 1987). Far from resonances it is indeed possible to reduce the full 27 components of the β tensor to ten independent components as a result of Kleinman permutation symmetry. There is good agreement between calculated values and those derived from X-ray experiment. For all methods β_{xxx} is the largest component and β_{xyy} is the second largest. However, the sign between the theoretical and experimental values differs. The component of β_{tot} calculated according to (9) and (11) are, respectively, $\beta_x = -42.3$, $\beta_y = 0.4$, $\beta_z = 7.2$ with $\beta_{\mathrm{tot}} = (\beta_x^2 + \beta_y^2 + \beta_z^2)^{1/2} = 42.9$. The components of β_{vec}, according to (8), are, respectively, $\beta_{x,\mathrm{vec}} = -39.12$, $\beta_{y,\mathrm{vec}} = 0.14$, $\beta_{z,\mathrm{vec}} = 1.10$ with $|\beta_{\mathrm{vec}}| = 39.14$; this value does not differ appreciably from β_{tot}. Thus, as expected, NPP belongs to the one-dimensional non-linear compounds, for which β_{xxx} is almost oriented along the dipole moment of the molecule. Components of the dipolar moment and modules of β_{tot} and β_{vec} are listed in Table 12, which also gives the angles between the vectors. The angle between $\boldsymbol{\beta}_{\mathrm{tot}}$ and $\boldsymbol{\mu}^D$ in NPP is only 19.8°. However, a molecule with a large non-linear optical response, but not oriented along the dipolar moment of the molecule, would give a wrong estimate of β when using EFISHG measurements (Meyers, Bredas & Zyss, 1992). Fig. 7 shows the dipolar moment vectors calculated by different methods; β_{tot} is also represented.

Conclusions

This paper has shown that an electron density study can yield estimates of the components of the quadratic non-linear susceptibility for anisotropic molecules and materials. It is also to be noted that contrary to theoretical estimation, the X-ray method evidences other significant components, namely:

(1) β_{xxy} and β_{yyy}, which indicate a strong departure from an idealized C_{2v} ($mm2$) molecular symmetry, with x as a hypothetical twofold axis.

(2) 'out-of-plane' β_{xxz}, β_{xzz} and β_{zzz} components, which point out the non-planar geometry,

Such differences are not surprising as quantum chemical calculations are performed on isolated molecules, whereas X-ray inferred values are indeed reflecting the influence of a strongly anisotropic environment. For real structures, other non-negligble components are an indication of the departure from such idealized geometry. Such symmetry-breaking effects can affect the π-electron system without actually distorting the nucleus backbone. Non-linear optical measurements in the crystal phase or the present X-ray electronic charge-diffraction technique are then sensitive probes of such crystal-field effects.

Combined X-ray and neutron measurements will become of particular relevance in systems with no sizeable dipole moments, for which classical EFISHG cannot be achieved. Furthermore, as discussed above, it will be possible to compare the values of T_{ijk} to those derived from harmonic Rayleigh scattering [HLS (Zyss, Chau Van, Dhenaut & Ledoux, 1993)], a promising new technique to investigate components of β in solution. An estimate of the influence of the crystal field (X-ray experiments in solid) or solvent effects in EFISHG or HLS measurements could be achieved by comparing the results of these methods.

A second question comes from the evaluation of the angle between $\boldsymbol{\mu}$ and $\boldsymbol{\beta}$. In poled polymers, where the non-linearity originates from oriented chromophores, the SHG or electrooptic coefficient is a higher-order Langevin function of $\boldsymbol{\mu}.\boldsymbol{\beta}$, which reflects the statistical ordering of the medium (Meyers *et al.*, 1992). Knowledge of $\boldsymbol{\mu}.\boldsymbol{\beta}$ is essential, but is hardly sufficient to obtain the magnitude of β in order to provide guidance for optimizing non-linear optical properties It is, therefore, essential to have direct access to values of the angle between $\boldsymbol{\mu}$ and $\boldsymbol{\beta}$, as in this work, or by theoretical means.

This research was supported by 'Centre National de la Recherche Scientifique'. The authors wish to thank J. Mainville for reading the manuscript.

References

ANDREAZZA, P., JOSSE, D., LEFAUCHEUX, F., ROBERT, M. C. & ZYSS, J. (1992). *Phys. Rev. B*, **45**, 7640–7649.

BAERT, F., SCHWEISS, P., HEGER, G. & MORE, M. (1988). *J. Mol. Struct.* **178**, 29–48.

BARZOUKAS, M., JOSSE, D., FREMEAUX, P. & ZYSS, J. (1987). *Non-linear Optical and Electroactive Polymers*, edited by P. N. PRASAD & D. R. ULRICH, pp. 69–103. New York, London: Plenum Press.

BARZOUKAS, M., JOSSE, D., FREMEAUX, P., ZYSS, J., NICOUD, J. F. & MORLEY, J. O. (1987). *J. Opt. Soc. Am. B*, **4**(6), 977–986.

BECKER, P. J. & COPPENS, P. (1974). *Acta Cryst.* A**30**, 129–147.

BLESSING, R. H. (1989). *J. Appl. Cryst.* **22**, 396–397.

CLEMENTI, E. (1965). Tables of atomic functions, supplement to IBM. *J. Res. Rev.* **9**, 2.

COPPENS, P. (1975) *Phys. Rev. Lett.* **34**, 98–100.

COPPENS, P., GURU ROW, T. N., LEUNG, P., STEVENS, E. D., BECKER, P. J. & YANG, Y. W. (1979). *Acta Cryst.* A**35**, 63–72.

COPPENS, P., LEISEROWITZ, L. & RABINOVICH, D. (1965). *Acta Cryst.* **18**, 1035–1038.

DOCHERTY, V. J., PUGH, D. & MORLEY, J. O. (1985). *J. Chem. Soc. Faraday Trans.* 2, **81**, 1179–1192.

DUNITZ, J. D., MAVERICK, E. F. & TRUEBLOOD, K. N. (1988). *Angew. Chem. Int. Ed. Engl.* **27**, 880–895.

DUNITZ, J. D., SCHOMAKER, V. & TRUEBLOOD, K. N. (1988). *J. Phys. Chem.* **92**, 856–867.

HANSEN, N. & COPPENS, P. (1978). *Acta Cryst.* A**34**, 909–921.

HIRSHFELD, F. L. (1976). *Acta Cryst.* A**32**, 239–244.

HIRSHFELD, F. L. (1977). *Theor. Chim. Acta*, **44**, 129–138.

JOHNSON, C. K. (1965). *ORTEP*. Report ORNL-3794. Oak Ridge National Laboratory, Tennessee, USA.

KANIS, D. R., RATNER, M. A. & MARKS, T. J. (1992). *J. Am. Chem. Soc.* **114**, 10338–10357.

LALAMA, S. J. & GARITO, A. F. (1979). *Phys. Rev. A*, **20**, 1179–1194.

LEDOUX, I. & ZYSS, J. (1982). *J. Chem. Phys.* **73**, 203–213.

MEYERS, F., BREDAS, J. L. & ZYSS, J. (1992). *J. Am. Chem. Soc.* **114**, 2914–2921.

OUDAR, J. L. (1977). *J. Chem. Phys.* **67**, 446–457.

PERIGAUD, A., GONZALES, F. & CUNISSE, M. (1991). *Ann. Chim. Fr.* pp. 133–141.

ROBINSON, F. N. H. (1967). *Bell. Syst. Tech. J.* pp. 913–956.

ROSENFIELD, R. E., TRUEBLOOD, K. N. & DUNITZ, J. D. (1978). *Acta Cryst.* A**34**, 828–829.

SCHOMAKER, V. & TRUEBLOOD, K. N. (1968). *Acta Cryst.* B**24**, 63–76.

SOUHASSOU, M., LECOMTE, C., BLESSING, R. H., AUBRY, A., ROHMER, M. M., WIEST, R., BENARD, M. & MARRAUD, M. (1991). *Acta Cryst.* B**47**, 253–266.

STEWART, R. F. (1973). *J. Chem. Phys.* **58**, 1668–1676.

STEWART, R. F., DAVIDSON, E. R. & SIMPSON, W. T. (1965). *J. Chem. Phys.* **43**, 175–187.

TEHRUNE, R. W., MAKER, P. D. & SAVAGE, C. M. (1965). *Phys. Rev. Lett.* **14**, 681–684.

TRUEBLOOD, K. N. (1990). *THMA*11. Univ. of California, Los Angeles, USA.

ZYSS, J. (1979*a*). *J. Chem. Phys.* **70**, 3333–3340.

ZYSS, J. (1979*b*). *J. Chem. Phys.* **70**, 3341–3349.

ZYSS, J. (1979*c*). *J. Chem. Phys.* **71**, 909–916.

ZYSS, J., CHAU VAN, T., DHENAUT, C. & LEDOUX, J. (1993). *Chem. Phys.* pp. 281–296.

ZYSS, J. & LEDOUX, I. (1994). *Chem. Rev.* **94**, 77–105.

ZYSS, J., NICOUD, J. F. & COQUILLAY, M. (1984). *J. Chem. Phys.* **81**, 4160–4167.

ZYSS, J. & OUDAR, J. L. (1982). *Phys. Rev. A*, **26**, 2028–2048.

Acta Cryst. (1995). B**51**, 209–220

An Extension of the *GROMOS* Force Field for Carbohydrates, Resulting in Improvement of the Crystal Structure Determination of α-D-Galactose

BY M. L. C. E. KOUWIJZER,* B. P. VAN EIJCK, H. KOOIJMAN AND J. KROON

Department of Crystal and Structural Chemistry, Bijvoet Center for Biomolecular Research, Utrecht University, Padualaan 8, 3584 *CH Utrecht, The Netherlands*

(*Received* 25 *May* 1994; *accepted* 3 *October* 1994)

Abstract

For carbohydrates the *GROMOS* force field has been extended to a more realistic all-atom model, with the use of parameters from the force field proposed by Ha, Giammona, Field & Brady [*Carbohydr. Res.* (1988), **180**, 207–221]. This extended and modified *GROMOS* force field has been used to simulate the crystal structures of seven monosaccharides. The results, compared with the experimental data, are satisfactory, and an overall improvement over those obtained with the comparable Ha force field. The experimentally determined positions of the H atoms should be used with caution in this comparison, and the thermal parameters can only be used as indicators for the preservation of the symmetry during the simulation. The simulations gave rise to suspicion about the hydroxyl H-atom positions in two of the sugars. These two structures were redetermined by X-ray diffraction at low temperature. For β-D-glucose essentially the same structure was found as in the original publication. In the case of α-D-galactose, the new structure confirmed the results from the simulation, in contrast to earlier experimental determinations.

* Author to whom all correspondence should be addressed.